Journal Pre-proof

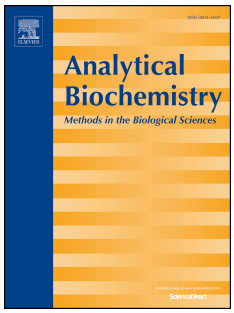

Electrochemical determination of uric acid in urine and serum with uricase/carbon nanotube /carboxymethylcellulose electrode

Toya Fukuda, Hitoshi Muguruma, Hisanori Iwasa, Takeshi Tanaka, Atsunori Hiratsuka, Tetsuo Shimizu, Katsumi Tsuji, Takahide Kishimoto

PII: S0003-2697(19)31087-5

DOI: https://doi.org/10.1016/j.ab.2019.113533

Reference: YABIO 113533

To appear in: *Analytical Biochemistry*

Received Date: 2 November 2019

Revised Date: 3 December 2019

Accepted Date: 4 December 2019

Please cite this article as: T. Fukuda, H. Muguruma, H. Iwasa, T. Tanaka, A. Hiratsuka, T. Shimizu, K. Tsuji, T. Kishimoto, Electrochemical determination of uric acid in urine and serum with uricase/carbon nanotube /carboxymethylcellulose electrode, *Analytical Biochemistry* (2020), doi: https://doi.org/10.1016/j.ab.2019.113533.

Toya Fukuda: Writing – Original Draft, Investigation, Data Curation, **Hitoshi Muguruma:** Conceptualization, Writing – Review & Editing, Formal analysis, **Hisanori Iwasa:** Methodology, **Takeshi Tanaka:** Methodology, **Atsunori Hiratsuka:** Validation, Project administration, Funding acquisition, **Tetsuo Shimizu:** Investigation, **Katsumi Tsuji:** Resources, Supervison, **Takahide Kishimoto:** Resources, Funding acquisition,

Graphical abstract

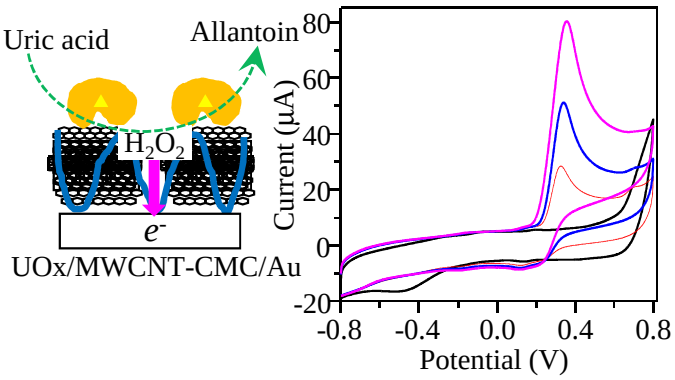

Electrochemical determination of uric acid in urine and serum with uricase/carbon nanotube /carboxymethylcellulose electrode

Toya Fukuda[a], Hitoshi Muguruma[a,b*], Hisanori Iwasa[b,c], Takeshi Tanaka[b], Atsunori Hiratsuka[a,b], Tetsuo Shimizu[b], Katsumi Tsuji[c], and Takahide Kishimoto[d]

[a]*Graduate School of Engineering and Science, Shibaura Institute of Technology, 3-7-5 Toyosu, Koto, Tokyo 135-8548, Japan.*

[b]*Nanomaterials Research Institute, National Institute of Advanced Industrial Science and Technology (AIST), Tsukuba Central 5-41, 1-1-1 Higashi, Tsukuba, Ibaraki 305-8565, Japan*

[c]*Research Center, Toyobo Co., Ltd. 2-1-1 Katata, Otsu, Shiga 520-0292, Japan*

[d]*Tsuruga Institute of Biotechnology, Toyobo Co., Ltd. 10-24 Toyo-cho, Tsuruga, Fukui 914-8550, Japan*

*Corresponding Author.

*****E-mail address: muguruma@shibaura-it.ac.jp (H. Muguruma).

Keywords:

Uric acid

Multi-walled carbon nanotube

Carboxymethylcellulose

Uricase

Biosensor

ABSTRACT

The detection of uric acid in blood and urine is clinically important in terms of suitable diagnosis and self-healthcare. An amperometric thin film biosensor composed of carbon nanotube and uricase enzyme is presented. The CNT is successfully dispersed in aqueous solution with carboxymethylcellulose surfactant. This enables thin film formation by a simple drop-casting layer-by-layer process. The uricase/carboxymethylcellulose dispersed carbon nanotube/gold thin film biosensor shows the best sensing performance compared to that with sodium cholate surfactant in terms of higher current and lower detection potential. The presented procedure shows good performance with neither electron transfer mediator nor complicated process. Cyclic voltammetry exhibited a sensitivity of 233 μA mM^{-1} cm^{-2} at +0.35 V, a linear range of 0.02-2.7 mM, and a detection limit of 2.8 μM. We quantify and graph uric acid data in actual physiological samples (serum and urine) for the first time and detection values showed good agreement with those obtained by a conventional analytical method (enzymatic colorimetry kit).

1. Introduction

Uric acid is the primary final product of purine metabolism, and it is released into blood serum or excreted by the kidneys in urine. Abnormal levels in blood and urine cause illnesses such as gout/arthritis, hyperuricaemia, kidney disease, Lesch-Nyhan syndrome, leukaemia, pneumonia, and renal dysfunction. The rapid detection of uric acid in blood and urine is clinically important: for example, alerting the presence of abnormal levels of uric acid allows concerned persons to take action (therapy) immediately. However, medical checkups, which often involve bulky apparatuses, laboratory setup, time, trained technicians, and pretreatment, do not meet this requirement.

High-performance liquid chromatography (HPLC) and spectroscopy are the present technique used. However, those require bulky equipment, sample pre-treatment, harmful solvent, skill, time, and cost. Thus, electrochemical analysis has many benefits overcoming drawbacks of conventional analytical methods, in fact, there have been many reports where the various modified electrodes are used [1-7]. However, a weak point of electrochemical methods is poor selectivity toward target agents. An electrochemical biosensor comprising a combination of uricase enzyme (urate oxidase, UOx) and transducer electrode entails many advantages in terms of simple operation procedure, low cost of the required equipment, high speed, and portability of the measurement system. UOx plays a role in chemical discrimination in the presence of many other chemicals. The performance of the electrochemical biosensor is dominated by the technique of enzyme immobilization onto the electrode. To date, nanomaterials-based uric acid biosensors have been reported [8-22]. In those, we notice that carbon nanotubes (CNT) lead to well-defined nanostructure, good electrocatalytic ability and electronic conductivity, and good connection between CNTs and enzymes [14-22]. However, there are two major requirements for realizing CNT-based enzyme biosensors. One is that the hydrophobic surface of the CNTs must be changed to a hydrophilic surface in order to be tuned with the enzyme environment. The other is how strongly aggregated CNT molecules are debundled for making use of CNT characteristics (large surface area, specific geometry).

Typical strategies for UOx immobilization with CNT-base electrodes are modification of nanoparticles [15-18], electron transfer mediators [19-22], and conductive polymers [21,22]. Our motivation is a simple and versatile procedure for practical use without metal or electron transfer mediator. We notice the formation of a thin film with drop-casting of a homogenous suspension of CNT. Here, we developed carboxymethylcellulose (CMC) as a surfactant for CNT dispersion in water. The CMC debundles CNTs by the electrostatic repulsion of the negatively charged molecules. As a result, the CNT dispersed solution with CMC as a surfactant is practicable for thin film fabrication on any type and shape of electrodes while maintaining the conductivity and catalytic ability of the CNTs. We have already reported the usefulness of the CNT-CMC electrode for electrochemical detection of catechins [23] and quercetins [24]. However, an enzymatic biosensor with CNT-CMC has not yet been explored. This is the first report of an amperometric biosensor composed of UOx and CNT-CMC thin film for quantifying uric acid in actual physiological samples such as serum and urine. The UOx/CNT biosensor with CMC exhibits the best sensing performance compared to that with the other surfactant, SC, in terms of higher current and lower detection potential. We quantify and graph uric acid data in actual physiological samples (serum and urine) for the first time and detection values showed good agreement with those obtained by a conventional analytical method (enzymatic colorimetry kit).

2. Experimental

2.1. Materials

UOx (EC. 1.7.3.3, from Bacillus sp., 1.5 U/mg) and uric acid measurement kit were developed by our group. Single-walled CNTs (SWCNTs, average diameter: 1.0 nm, length: 5-10 μm) produced by enhanced direct injection pyrolytic synthesis [25] were purchased from Meijo Nano Carbon Co., Ltd. (Nagoya, Japan). Multi-walled CNTs (MWCNTs, average diameter: 9.5 nm, average length: 1.5 μm) were purchased from Nanocyl S. A. (Sambreville, Belgium). Sodium cholate (SC), uric acid, urea, and ascorbic acid were purchased from Kanto Chemical Co., Inc.

(Tokyo, Japan). CMC, Nafion, and potassium hexacyanoferrate(II, III) ($K_4[Fe(CN)_6]$, $K_3[Fe(CN)_6]$) were purchased from Aldrich (St. Louis, USA). Control serum (I wako/BR) was purchased from Wako (Osaka, Japan).

2.2. Dispersion of CNTs

The electrode was formed on evaporated gold on a plastic substrate. The area of the opening for the working electrode was 9 mm^2. CNT dispersion processes with SC [26] and CMC [23] are described in the literature. The optimum conditions for CNT dispersion in water were SWCNT/SC: 0.1/2.0%, SWCNT/CMC: 0.1/0.3%, MWCNT/SC: 0.1/2.0%, and MWCNT/CMC: 0.1/0.05%. Fig. S1 (Supplementary data) presents the optical absorption spectra of CNT-CMC and CNT-SC dispersed aqueous solutions.

2.3. Electrode preparation

Aliquots (3–5 μL) of the CNT-CMC and CNT-SC solutions were dropped onto the Au surface and dried. Then, 3-10 μL aliquots of enzyme (5 U) in phosphate buffer (50 mM, pH 7.4) were dropped onto the surface. Finally, 5 μL aliquots of 1.0% Nafion solution were dropped onto the surface. Outer membrane Nafion plays a role as an immobilization matrix for UOx and CNTs. For simple expression, the description of “Nafion” is omitted.

2.4. Measurements

Atomic force microscopy (AFM) was conducted in tapping mode in the ambient atmosphere using a commercial AFM system (Park Systems NX10 AFM). The scanning tip was a silicon cantilever. Electrochemical measurements were performed with an electrochemical analyser (ALS Instruments, 701A West Lafayette, IN, USA) using a three-electrode configuration. Reference (Ag/AgCl saturated KCl, RE-1C) and counter (platinum wire) electrodes were purchased from BAS Inc. (Tokyo, Japan). Electrochemical measurements were conducted in a 5 mL vessel at 20 °C using a phosphate buffer (50 mM, pH 7.4) as the supporting electrolyte, to which stock uric acid solutions of 5 mM were successively added to prepare samples with designated concentrations.

3. Results and Discussion

3.1. Optimization of UOx/CNT electrode

We tested both SWCNTs and MWCNTs. The SWCNTs were formed by rolling a single graphite sheet, whereas the MWCNTs were composed of several coaxial shells of SWCNTs. The primary difference parameter between SWCNTs and MWCNTs is diameter. Typical SWCNT diameter is 1-2 nm, whereas that of MWCNT is at least 10 nm. For comparison, we test two surfactants: CMC (anionic polymer) and SC (anionic low molecular mass compound). Both are anionic surfactants. The difference is molecular mass. SC is a low molecular mass compound, whereas CMC is a macromolecule. SC is widely used as a surfactant for CNT dispersion for enzyme biosensor applications [27-29]. Figs. 1A and S2 (Supplementary data) show cyclic voltammetry (CV) results for uric acid on UOx/Au (control), CNT-CMC/Au (control), UOx/SWCNT-SC/Au, UC/SWCNT-CMC/Au, UOx/MWCNT-SC/Au, UOx/MWCNT-CMC/Au, and UOx/CNT/Au (control). Anodic peak currents at 0.4-0.6 V (see arrows in Fig. 1A) are due to uric acid reactions observed at all electrodes. There was no distinct peak for the UOx/Au electrode (no CNT, black lines in Fig. 1A and S2A), and there was no peak for the CNT-CMC/Au electrode (Fig. S2B), indicating the effectiveness of UOx and CNT. The current response originates from the fact that UOx specifically catalyses the oxidation of uric acid according to the following equation:

$$\text{Uric acid} + O_2 + H_2O \xrightarrow{\text{UOx}} \text{Allantoin} + CO_2 + H_2O_2, \qquad (1)$$

and CNT catalyses the reaction of hydrogen peroxide according to the following equation:

$$H_2O_2 \rightarrow 2H^+ + O_2 + 2e^-. \qquad (2)$$

The current increases as the Au anode receives electrons. The reason why the gold is used is that its surface is relatively clean and inert, in a work, less catalytic ability. Therefore, the increment current can be attributed to the catalytic ability of CNT. We confirmed that UOx/MWCNT-CMC/carbon paste electrode showed the similar sensing performance with Au. Whether we use carbon paste and gold, it does not affect the result. Using CNT is critical. The peak current of the

CNT-CMC electrode is larger than that of CNT-SC. The peak potential position of the CNT-CMC electrode is smaller than that of CNT-SC. Those tendencies are independent of CNT type. Fig. S3 (Supplementary data) shows UOx of potassium hexacyanoferrate on UOx/Au, UOx/SWCNT-SC/Au, UOx/SWCNT-CMC/Au, UOx/MWCNT-SC/Au, and UC/MWCNT-CMC/Au electrodes. The redox peak pairs are assigned to potassium hexacyanoferrate(II) and (III), which react at the CNT-surfactant layer. The fact that the peak potential position of the CNT-CMC electrode is smaller than that of CNT-SC mirrors the CV profiles of uric acid in Fig. 1A and Fig. S2C-F. The reason why peak potential of UOx/MWCNT-SC/Au electrode is massive than the peak potential of UOx/MWCNT-CMC/Au electrode is due to the overpotential. The surfactant at CNT surface disturbs the electrochemical oxidation and amount of surfactant of UOx/MWCNT-SC/Au electrode is larger than that of UOx/MWCNT-CMC/Au. It is related with catalytic ability for oxidation of hydrogen peroxide, consequently the peak potential increased and the peak current of SC using electrode decreased compared to CMC using electrode. Therefore, amount ration between CNT and surfactant needs to be optimized (discuss following).

Potassium hexacyanoferrate can be used as a redox marker during the conduction of electrochemical impedance spectroscopy (EIS). Fig. 1B and 1C show EIS results for investigating the electron transfer properties of UOx/SWCNT-SC/Au, UOx/SWCNT-CMC/Au, UOx/MWCNT-SC/Au, and UOx/MWCNT-CMC/Au electrodes with different representation for scale. In those Nyquist plots, the electron transfer resistance of CNT-CMC, which is represented by the diameter of the semicircle at high frequencies, is much smaller than that of CNT-SC. The low-frequency straight line of both MWCNT-CMC and SWCNT-CMC electrode is 45º. This means that the surface is uniform and it is the best electrode. The other electrode surfaces are not uniform probably because the CNT dispersion is insufficient. The electron transfer exhibits a strong correlation with CV.

When the surfactant amount is too small, debundling is insufficient. When the surfactant amount is too high, the surfactant disturbs conveyance of the electronic signal. In both cases, the

sheet and/or electron transfer resistance of the CNT film also become higher. The optimum mass ratio range of [CNT]/[CMC] is 0.5-3 [30], which is smaller than those obtained with [CNT]/[SC] (=20) [27]. The electrode without surfactant (UOx/MWCNT/Au, Fig. S2G) showed inferior characteristics compared with that with surfactant (UOx/MWCNT-CMC/Au and UOx/MWCNT-SC/Au). In a word, the peak potential is larger and the peak current is smaller comparing. This demonstrates the effect of the CNT dispersion with surfactant. The surfactant contributes the thin film formation but also provides hydrophilic environment for enzyme immobilization. Dispersion by CMC is the most efficient for thin film formation while maintaining the conductivity and catalytic ability of the CNTs. Furthermore, the biosensor with CNT-CMC shows the better electrocatalytic performance towards hydrogen peroxide than does the SC counterpart. Dispersion by CMC enhances the active surface area and forms conductive networks: consequently, electron conductivity and electrocatalytic ability are accelerated. Since CMC is polymer material, the immobilization is available for any type of surfaces including gold. This is also the advantage of CNT-CMC electrode.

It is concluded that CMC is the best material for CNT dispersion for fabrication of the enzymatic uric acid biosensor. This is the first report on an enzymatic biosensor with CNT-CMC dispersed solution. The following experiment is conducted using UOx/MWCNT-CMC/Au electrode as a biosensor.

The property of enzyme-based biosensors is often affected by the environmental pH. The pH depemdence of pH was investigated in 0.87 mM uric acid solution at +0.35 V over the pH range from 6.0 to 9.0 as shown in Fig S4 (Supplementary data). It can be seen that response current increases with increasing pH value from 6.0 to 8.0. The current decreased over when pH reached 9.0. This tendency is similar with free UOx [31], suggesting that natural state of enzyme is retained with immobilization process. Since the purpose of this research is uric acid quantification in real physiological sample, the following experiment is conducted at pH 7.4.

3.2. Uric acid sensing performance

One of the advantages of our procedure is that it can be conducted with a simple drop casting layer-by-layer process. We evaluate each stage of this process with AFM images, where Figs. 2A, 2B, and 2C show MWCNT-CMC, UOx/MWCNT-CMC, and Nafion/UOx/MWCNT-CMC, respectively. In Fig. 2A, tubular and web structures are observed. This indicates that the MWCNTs are well dispersed and that the individual MWCNTs form networks with tube-tube junctions. The thinnest fibre-like structure we can observe has an average width of 26 nm (see arrow in Fig. 2A), which is larger than the average diameter of an individual MWCNT molecule. This is because the AFM tip used is outside the resolution limit for objects in the horizontal direction. To the contrary, the step height due to the cross-sectional profile concisely expresses the diameter (ca. 10 nm) of the MWCNT. This is the evidence that CNT debundling is achieved. In Fig. 2B, the tubular structure disappeared because UOx covers the CNT networks. Instead, globular shapes are observed (see arrow in Fig. 2B). Those shapes are probably clusters of UOx molecules because the dimension of UOx molecules is several nanometers. The profile and roughness in Fig. 2C are similar with those of Fig. 2B. AFM observation indicates that layer-by-layer casting is adequately completed.

The effects of the potential scan rate on the CV response for potassium hexacyanoferrate (Fig. 3A) and uric acid (Fig. 3B) were examined from 10 to 500 mV s^{-1}. In Fig. 3A, redox peak pairs (E_{pa}=+0.29 V and E_{pc}=+0.15 V) are assigned to the redox reactions between potassium hexacyanoferrate(II) and (III). The ratio of the cathodic to anodic current (I_{pc}/I_{pa}) is close to 1, and an observed peak-to-peak potential separation (ΔE_p) was estimated as 90 mV, which was within range for a reversible process. The I_p values are plotted against the square root of scan rate ($v^{1/2}$) in Fig. 3C. The linear relationship between I_p and $v^{1/2}$ corresponds to a diffusion-controlled redox process. It can best be described by the Randles-Sevcik equation as follows:

$$I_p=269n^{3/2}ACD^{1/2}\,v^{1/2} \qquad (3)$$

where n is the number of transferred electrons, A is the surface area of the electrode (cm^2), C is the molar concentration of redox chemicals (mol/L), and D is the diffusion coefficient ($cm^2\ s^{-1}$). Using

Eq. (3), the *D* values for the redox processes (potassium hexacyanoferrate marker) at UOx/MWCNT-CMC/Au electrodes were estimated as 3.4×10^{-6} cm^2 s^{-1}. The peak currents of the redox system were proportional to the scan rate at higher scan rates (> 150 mV s^{-1}), indicating a limitation due to the electron transfer kinetics. In this region, the peak separation increases, indicating that the surface reaction becomes irreversible with increasing scan rate. For an irreversible electrode reaction, the relationship between peak potential and scan rate follows Laviron's law [32]. The standard rate constant of the surface reaction of marker ion is estimated as 1.1 s^{-1} from the I_p vs. log ν plot shown in Fig. S5 (Supplementary data).

In Fig. 3B, the anodic peak (E_{pa}=+0.35 V) is assigned to the oxidation of hydrogen peroxide generated by uric acid oxidation by UOx. In the cathodic scan, there is no distinctive peak, which indicates that the oxidation of hydrogen peroxide is irreversible. The anodic peak current is proportional to the square root of the scan rate, which indicates that the oxidative current is controlled by the diffusion of uric acid from the bulk solution to the electrode surface in the range of 10-150 mV s^{-1}. When ν exceeds 150 mV s^{-1}, I_p is proportional to ν, which indicates that the oxidative current is a surface-controlled process. From the obtained results, a scan rate of 50 mV s^{-1} was selected for the following analytical experiments. The *D* values for uric acid at UOx/MWCNT-CMC/Au electrodes were estimated at 2.2×10^{-6} cm^2 s^{-1}. This value is smaller than that of the redox marker potassium hexacyanoferrate. The electrochemical response is dominated by the diffusion of uric acid.

The catalytic rate constants (k_{cat}) of UOx/MWCNT-CMC/Au electrodes were estimated by chronoamperometry, as shown in Fig. S6A (Supplementary data). k_{cat} was calculated using Galus's method [33]:

$$I_C/I_L = (\pi k_{cat} C t)^{1/2} \qquad (4)$$

where I_C is the catalytic current of uric acid at UOx/MWCNT-CMC/Au electrodes, I_L is the limited current in the absence of uric acid, *C* is uric acid concentration, and *t* is the time elapsed. The slope

of the representation of I_C/I_L vs. $t^{1/2}$ for 3.8 mM uric acid (Fig. S6B, Supplementary data) allowed us to estimate the catalytic constant k_{cat} as 5.3×10^3 M^{-1} s^{-1} at UOx/MWCNT-CNT/Au electrodes.

Figure 4A shows CV results of various uric acid concentrations of physiological level at UOx/MWCNT-CMC biosensor electrode. Uric acid concentration-dependent current of +0.35 V was observed. This is attributed to the oxidation of hydrogen peroxide caused by enzymatic reaction of uric acid. Figure 4B shows the time-current traces at fixed potential of various uric acid concentrations of physiological level at UOx/MWCNT-CMC biosensor. A sequential increase in uric acid concentration at regular intervals is observed. The response time was 7 s. The step shape shows ideal sensing response. The effects of the interfering compounds urea and ascorbic acid at physiological levels on the sensing characteristics are negligible (inset of Fig. 4B). Figure 4C shows the plot of current vs. uric acid concentration based on the data from Fig. 4A and 4B. The sensitivity determined from the slopes for the UOx/MWCNT-CMC/Au biosensor was 233 μA mM^{-1} cm^{-2} (r = 0.999 in the linear range of 0.02-2.7 mM) by CV and 356 μA mM^{-1} cm^{-2} (r = 0.999 in the linear range of 0.02-1.2 mM) by time-current measurement. The limit of detection (LOD) and limit of quantification (LOQ) for uric acid were calculated by using the following formula, LOD=3 S/M and LOQ=10 S/M (where S is the standard deviation of blank and M is the slope of the calibration plot [7]), obtained values of LOD and LOQ of CV (time-current measurement) were 2.8 (1.8) μM and 9.3 (6.1) μM, respectively. The dynamic range obtained by CV is larger than that of time-current measurement. Normal ranges of uric acid in human body fluids are 0.1-0.4 mM in blood and 1.5-4.4 mM in urine [2]: therefore, the UOx/MWCNT-CMC/Au biosensor can be applied for mediator-free, noninvasive, and point-of-care detection of uric acid from serum and urine. The reproducibility of CV is also better than that of time-current measurement, probably because CV scanning includes the electrode cleaning effect, which enhances reproducibility.

The reaction at the sensing surface is systematically discussed. We consider the following reaction sequence presented as:

$$\text{Substrate}_{\text{bulk}} \xrightarrow{k_D} \text{Substrate}_{\text{surface}} + \text{UOx} \xrightarrow{K_M} \text{UOx-Substrate} \xrightarrow{k_C} \text{UOx} + \text{Products} \quad (5).$$

where k_D denotes the rate constant for mass transport from solution (bulk) to the sensing surface, K_M denotes the Michaelis constant, and *k*c denotes the catalytic rate constant. The substrate is free to diffuse through the film with a diffusion coefficient *D*, which is generally proportional to k_D. Actual analytical information (current) is proportional to $D \times C$, where *C* is substrate concentration. For concentrations within the detectable linear range (0.020-2.7 mM), the diffusion control condition is maintained: consequently, quantification is valid. Saturation is observed from linearity at higher (>3.0 mM) uric acid concentrations, which represents a typical characteristic of the Michaelis-Menten model. This is a reaction-controlled step and can be applied to the Michaelis-Menten analysis, i.e., the Lineweaver-Burk plot (double reciprocal plot), based on the following equation:

$$\frac{1}{I} = \frac{K_M^{app}}{I_{max}} \frac{1}{C} + \frac{1}{I_{max}} \quad (6).$$

K_M^{app} denotes the apparent Michaelis constant and is estimated to be 0.63 mM, which is similar to values for other uric acid biosensors [10]. The 0.63 mM K_M^{app} of the sensor is larger than that of free UOx (K_M=0.0136 mM). This is attributed to the fact that the layer-by-layer thin film biosensor is set for diffusion control to detect the physiological uric acid.

A comparison of the performances of the fabricated biosensors compared with those of other uric acid CNT-based biosensors is shown in Table 1, indicating that the present sensor exhibited similar or better performance compared with the other reported biosensors. It should be emphasized that our method is conducted without the external electron transfer mediator, which involves some disadvantages: (i) the process for mediator immobilization is complicated, including the preparation of an accommodating polymer matrix and requiring fine-tuning between a hydrophobic mediator and a hydrophilic enzyme, which is not avoidable; (ii) leaching of the free mediators also reduces the sensitivity, and even causes poisoning problems. Our method is also performed without nanoparticles. Therefore, the proposed dry chemical process for fabrication of a biosensor is simple and versatile.

3.3. Uric acid determination in actual physiological samples

Measurement of actual samples is conducted. The control serum is used as a model of a blood sample. For comparison, the uric acid concentrations are independently measured by an enzymatic colorimetry kit. UOx is also used in this kit. First, the specimen (serum or urine) is reacted by UOx as in Eq (1). Subsequently, the generated hydrogen peroxide is reacted with 4-aminoantipyrine (4-AA) and N-ethyl-N-(3-sulfopropyl)-m-anisidine (ESPAS) by peroxidase (POx) enzyme as follows:

$$2H_2O_2 + 4\text{-AA} + \text{ESPAS} \xrightarrow{\text{POx}} \text{quinone colour } (\lambda = 540 \text{ nm}) + 4H_2O \qquad (7).$$

Fig. 5A shows the CV results of control serum containing various concentrations of uric acid. The uric acid dependent oxidative currents (see asterisk in Fig. 5A) are observed at +0.35 V. The current increment at approximately +0.25 V is due to electrochemical agents containing serum. This does not affect the quantification of uric acid. Urine is also a typical human fluid. The concentration range of uric acid in urine is relatively large. In some cases, the level of uric acid surpasses the linear range of the biosensor. Therefore, the measurement is conducted after dilution. Fig. 5B exhibits CV results of urine of a young man at various dilutions. Uric acid measurements were conducted for 4 young men whose ages were mid-20s. The CV profiles of Fig. 5B are similar to those of Fig. 4A, indicating that a major ingredient in urine is uric acid. Figure 5C shows a plot of biosensor values (detection current) and enzymatic colorimetry kit values of various serum and urine samples. They have strong correlations with the fitting line based on their simulated CV results (Fig. 4C). There is good agreement between the values obtained by biosensor and enzyme colorimetric kit. The correlation coefficient is 96.3%, suggesting that the present biosensor can be used for uric acid measurement and demonstrated excellent precision, accuracy, and reliability in practical application. It is remarkable that we presented graph uric acid data in actual physiological samples (serum and urine) for the first time. Previous reports presented only numbers, not graphs. Therefore, we emphasize the excellent performance of UOx/MWCNT-CMC biosensors.

It should be emphasized that we present the raw data of real samples, in contrast to many reports which presented only numbers: not raw data, as in our presentation. This is solid evidence

for the effectiveness of our biosensor. For example, if the sample is not urine or serum, we can immediately notice invalid data from CV profiles. This is thought to be difficult with amperometry at fixed potential, because it yields only mere numbers. Furthermore, CV is advantageous for this purpose because a repeat scan can enhance the reproducibility through stability of the electron transfer rate and the cleaning effect of the electrode surface. Fig. S7 (Supplementary data) shows repeated measurements of urine with the same biosensor, indicating that the biosensor exhibits good repeatability: the response for the five repeat measurements exhibited less than 5% signal loss. The reproducibility of from sample to sample (n=5) gave a standard deviation of 1.3%. The storage stability of the electrode was studied over a period of 10 days by storing it in buffer at 4 ºC and recording the current (at +0.35 V in the presence of 0.5 mM uric acid) in 2-day intervals. Fig. S8 (Supplementary data) shows continuous operation polarization at +0.35 V in the presence of 0.41 mM uric acid. The signal is kept at 90% of the initial current after 24 h.

4. Conclusion

An amperometric thin film biosensor composed of CNT-CMC and UOx enzyme is presented. CNT is successfully dispersed in aqueous solution with CMC surfactant. This enables thin film formation by a simple drop casting layer-by-layer process. The UOx/CNT biosensor with CMC exhibits the best sensing performance compared to that with the other surfactant, SC, in terms of higher current and lower detection potential. CV and time-current measurement at fixed potential exhibited sensitivity values of 233 and 356 μA mM^{-1} cm^{-2} at +0.35 V vs. Ag/AgCl, linear ranges of 0.02-2.7 and 0.02-1.2 mM, and detection limits of 2.8 and 1.8 μM. Detection values for actual physiological samples (serum and urine) showed good agreement with those obtained by a conventional analytical method (enzymatic colorimetry kit). These results will contribute to sustainable life as a point-of-care device. The procedure may be easily extended to other biosensors.

Declaration of interests

The authors declare that they have no known competing financial interests or personal relationships that could have appeared to influence the work reported in this paper.

Appendix A. Supplementary data

Supplementary data associated with this article can be found in the online version at http://dx.doi.org/xx.xxxx/j.ab.xxx.xx.xxx.

References

[1] J. G. Manjunatha, Poly(nigrosine) modified electrochemical sensor for the determination of dopamine and uric acid: a cyclic voltammetric study, Inter. J. ChemTehc Res. 9 (2016) 136-146.

[2] J. G. Manjunatha, Electrochemical polymerised graphene paste electrode and application to catechol sensing, Open Chem. Eng. J. 13 (2019) 81-87.

[3] A New electrochemical sensors based on modified carbon nanotube-graphene mixture paste for voltammetric determination of resorcinol, Asian J. Pharm. Clin. Res. 10 (2017) 295-300.

[4] J. G. G. Manjunatha, A novel poly (glycine) biosensor towards the detection of indigo carmine: A voltammetric study, J. Food Drug Anal. 26 (2018) 292-299.

[5] J. G. Manjunatha, Electroanalysis of estriol hormone using electrochemical sensor, Sens. Bio-Sensing Res. 16 (2017) 79-84.

[6] J. G. Manjunatha, A novel voltammetric method for the enhanced detection of the food additive tartrazine using an electrochemical sensor, Heliyon 4 (2018) e00986.

[7] N. Hareesha, J. G. J. G. Manjunatha, C. Raril, G. Tigari, Design of novel surfactant modified carbon nanotube paste electrochemical sensor for the sensitive investigation of tyrosine as a pharmaceutical drug, Adv. Pharm. Bull. 9 (2019) 132-137.

[8] S. Verma, J. Choudhary, K.P. Singh, P. Chandra, S.P. Singh, Uricase grafted nanoconducting matrix based electrochemical biosensor for ultrafast uric acid detection in human serum samples, Inter. J. Biol. Macromol. 130 (2019) 333-341.

[9] S. Jain, S. Verma, S.P. Singh, S.N. Sharma, An electrochemical biosensor based on novel butylamine capped CZTS nanoparticles immobilized by uricase for uric acid detection, Biosens. Bioelectron. 127 (2019) 135-141.

[10] K. Jindala, M. Tomar, V. Gupta, A novel low-powered uric acid biosensor based on arrayed p-njunction heterostructures of ZnO thin film and CuO microclusters, Sens. Actuators B 253 (2017) 566-575.

[11] M. N. Omar, A.B. Salleh, H. N. Lim, A. A. Tajudin, Electrochemical detection of uric acid via uricase-immobilized graphene oxide, Anal. Biochem. 509 (2016) 135-141.

[12] R. Ahmada, N. Tripathy, N. K. Jang, G. Khang, Y.-B. Hahn, Fabrication of highly sensitive uric acid biosensor based on directly grown ZnO nanosheets on electrode surface, Sens. Actuators B 206 (2015) 146-161.

[13] R. Devi, C.S. Pundir, Construction and application of an amperometric uric acid biosensor based on covalent immobilization of uricase on iron oxidenanoparticles/chitosan-γ-polyaniline composite film electrodeposited on Pt electrode, Sens. Actuators B 193 (2014) 608-615.

[14] Z. Herrastia, F. Martíneza, E. Baldrich, Detection of uric acid at reversibly nanostructured thin-film microelectrodes, Sens. Actuators B 234 (2016) 667-673.

[15] D. Chen, Q. Wang, J. Jin, P. Wu, H. Wang, S. Yu, H. Zhang, C. Cai, Low-potential detection of endogenous and physiological uric acid at uricase-thionine-single-walled carbon nanotube modified electrodes, Anal. Chem. 82 (2010) 2488-2455.

[16] L. Sun, J. Liu, P. Zhang, Y. Meng, C. Liu, Y. Ma, Q. Xie, W. Meng, An amperometric biosensor and a biofuel cell of uric acid based on a chitosan/uricase–poly(furan-3-boronic acid)–Pd nanoparticles/plated Pd/multiwalled carbon nanotubes/Au electrode, J. Electroanal. Chem. 739 (2015) 187-196.

[17] M.E. Ghica, C.M.A. Brett, Poly(brilliantgreen) and poly(thionine) modified carbon nanotube coated carbon film electrodes for glucose and uric acid biosensors, Talanta 130 (2014) 198-206.

[18] P.E. Erden, C. Kaçar, F. Öztürk, E. Kılıç, Amperometric uric acid biosensor based on poly(vinylferrocene)-gelatin-carboxylated multiwalled carbon nanotube modified glassy carbon electrode, Talanta 134 (2015) 488-495.

[19] N. Chauhan, C.S. Pundir, An amperometric uric acid biosensor based on multiwalled carbon nanotube–gold nanoparticle composite, Anal. Biochem. 413 (2011) 97-103.

[20] A. Numnuam, P. Thavarungkul, P. Kanatharana, An amperometric uric acid biosensor based on chitosan-carbon nanotubes electrospun nanofiber on silver nanoparticles, Anal. Bioanal. Chem. 406 (2014) 3763-3772.

[21] R. Rawal, S. Chawla, N. Chauhan, T. Dahiya, C.S. Pundir, Construction of amperometric uric acid biosensor based on uricase immobilized on PBNPs/cMWCNT/PANI/Au composite, Inter. J. Biol. Macromol. 50 (2012)112-118.

[22] K. Arora, M. Choudhary, B.D. Malhotra, Enhancing performance of uricase using multiwalled carbon nanotube doped polyaniline, App. Biochem. Biotechnol. 174 (2014) 1174-1187.

[23] H. Muguruma, S. Murakami, S. Takahashi, N. Osakabe, H. Inoue, T. Ohsawa, Separationless and adsorptionless quantification of individual catechins in green tea with a carbon nanotube-carboxymethylcellulose electrode, J. Agri. Food Chem. 67 (2019) 943-954.

[24] S. Takahashi, H. Muguruma, N. Osakabe, H. Inoue, T. Ohsawa, Electrochemical determination with a long-length carbon nanotube electrode of quercetin glucosides in onion, apple peel, and tartary buckwheat, Food Chem. 300 (2019) 125189.

[25] T. Saito, S. Ohshima, T. Okazaki, S. Ohmori, M. Yumura, S. Iijima, Selective diameter control of single-walled carbon nanotube in the gas-phase synthesis, J. Nanosci. Nanotechnol. 8 (2008) 6153-6157.

[26] M. Shimizu, S. Fujii, T. Tanaka, H. Kataura, Effects of surfactants on the electronic transport properties of thin-film transistors of single-wall carbon nanotubes, J. Phys. Chem. C 117 (2013) 11744-11749.

[27] H. Muguruma, H. Iwasa, H. Hidaka, A. Hiratsuka, H. Uzawa, Mediatorless direct electron transfer between flavin adenine dinucleotide-dependent glucose dehydrogenase and single-walled carbon nanotubes, ACS Catal. 7 (2017) 725-734.

[28] J. Chen, T.O. Tran, M.T. Ray, D.B. Brunski, J.C. Keay. D. Hickey, M.B. Johnson, D.T. Glatzhofer, D.W. Schmidtke, Effect of surfactant type and redox polymer type on single-walled carbon nanotube modified electrodes, Langmuir 29 (2013) 10586-10595.

[29] T.-W. Tsai, G. Heckert, L.F. Neves, Y. Tan, D.-Y. Kao, R.G. Harrison, D.E. Resasco, D.W. Schmidtke, Adsorption of glucose oxidase onto single-walled carbon nanotubes and its application in layer-by-layer biosensors, Anal. Chem. 81 (2009) 7917-7925.

[30] H. Muguruma, Y. Inoue, H. Inoue, T. Ohsawa, Electrochemical study of dopamine at electrode fabricated by cellulose-assisted aqueous dispersion of long-length carbon nanotube, J. Phys. Chem. C 120 (2016) 12284-12292.

[31] S. Asano, K. Yamamoto, S. Terashima, T. Kikuchi, Y. Kawamura, Study of a liquid type reagent for determination of uric acid by using thermostable recombinant uricase, Rinsho Kagaku 23 (1994) 214-220.

[32] E. Laviron, General The use of linear potential sweep voltammetry and of A.C. voltammetry for the study of the surface electrochemical reaction of strongly adsorbed systems and of redox modified electrodes, J. Electroanal. Chem. 100 (1979) 263-270.

[33] Z. Galus, Fundamentals of Electrochemical Analysis, Ellis Horwood, New York, 1976.

Figure captions

Fig. 1. (A) CV profiles of various UOx/CNT electrodes: UOx/Au (black), UOx/SWCNT-SC/Au (light blue), UOx/MWCNT-SC (red), UOx/SWCNT-CMC/Au (blue), and UOx/MWCNT-CMC (green). Uric acid concentration is 3.8 mM. Sweep rate: 50 mV s^{-1} in pH 7.4, 50 mM phosphate buffer solution. (B,C) Nyquist plots of the various UOx/CNT electrodes as in (A). The electrolyte was pH 7.4, 50 mM phosphate buffer solution containing 10 mM $K_3[Fe(CN_6)]/K_4[Fe(CN)_6]$ (1:1).

Fig. 2. AFM images of (A) MWCNT-CMC, (B) UOx/MWCNT-CMC, and (C) Nafion/UOx/MWCNT-CMC. Horizontal scale: 1×1 mm, Vertical scale: (A) 125 nm, (B) 200 nm, and (C) 200 nm.

Fig. 3. CVs of (A) 3.8 mM uric acid and (B) 10 mM $K_3[Fe(CN_6)]/K_4[Fe(CN)_6]$ (1:1) with the UC/MWCNT-CMC Au electrode at various scan rates. Scan rates: 0.01, 0.025, 0.05, 0.10, 0.15, 0.30, and 0.50 V s^{-1}. (C) Dependence of peak current on square root of potential sweep rate with electrolyte in 50 mM phosphate buffer solution at pH 7.4.

Fig. 4. (A) CV and (B) effects of interfering compounds with respect to the UOx/SWCNT-CMC/Au electrode. Sweep rate: 50 mV s^{-1}. Uric acid concentrations of 0, 0.020, 0.050, 0.10, 0.19, 0.28, 0.41, 0.58, 0.87, and 1.2 mM in pH 7.4 phosphate buffer solution (B). Inset: The effects of interferent species (0.1 mM urea (UR) and 0.1 mM ascorbic acid (AA)). The sequential concentrations of uric acid (UA) were 0.1, 0.2, and 0.4 mM. The polarization potential was +0.35 V vs. Ag/AgCl with an electrolyte of pH 7.4, 50 mM phosphate buffer solution. (C) Calibration plot for uric acid response using the data in 4A and 4B. The sensitivities of the electrodes were 233 μA mM^{-1} cm^{-2} (r = 0.999 in the linear range of 0.020-2.7 mM) by CV and 356 μA mM^{-1} cm^{-2} (r = 0.999 in the linear range of 0.020-1.2 mM) by CV.

Fig. 5. (A) CV of serum sample. Uric acid concentrations of 0.28, 0.37, 0.46, and 0.63 mM. Sweep rate: 50 mV s^{-1}. (B) CV of urine sample with various dilutions. Raw urine concentration was 2.5 mM. Sweep rate: 50 mV s^{-1} in pH 7.4 phosphate buffer solution. (C) Plot of biosensor values

(detection current) and enzymatic colorimetry kit values of various serums and urines. The fitting line is based on the standard sample in Fig. 4C.

Table 1
Comparison of the performance parameters of CNT-base uric acid biosensors.

biosensor	Detection potential (V)	Sensitivity ($\mu AmM^{-1}cm^{-2}$)	Linear range (mM)	Detection limit (μM)	ref
UOx/MWCNT-CMC/Au	0.35	233	0.02-5.0	2.8	This work
Magnetically entrapped SWCNT	N/A	N/A	0.001-0.20	0.83	(14)
UOx-Thionine-SWCNT	0.40	90	0.002-2.0	0.5	(15)
CS/UOx-PFBA-PdNPs/Pd/MWCNT/Au	0.55	490	0.001-2.5	0.1	(16)
UOx/PBG/MWCNT/CFE	0.30	248	0.002-0.1	0.6	(17)
PVF-c-MWCNT-GEL	0.50	N/A	0.0002-0.71	0.023	(18)
UOx/AuNP/c-MWCNT/Au	0.50	N/A	0.01-0.8	10	(19)
PBNPs/c-MWCNT/PANI	0.40	N/A	0.005-0.8	5	(20)
UOx-PANI-MWCNT/ITO	0.45	43.2	0.01-1.0	10	(21)

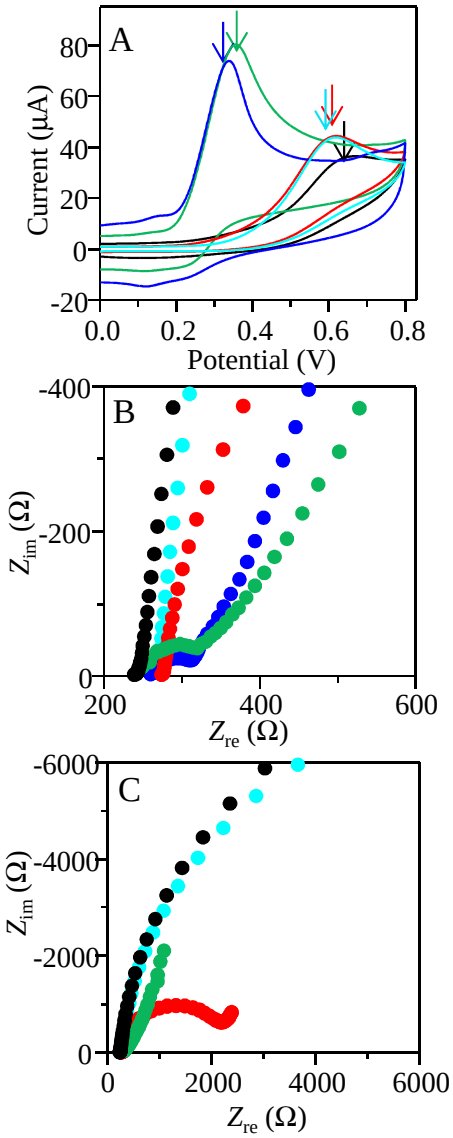

Fig. 1. (A) CV profiles of various UOx/CNT electrodes: UOx/Au (black), UOx/SWCNT-SC/Au (light blue), UOx/MWCNT-SC (red), UOx/SWCNT-CMC/Au (blue), and UOx/MWCNT-CMC (green). Uric acid concentration is 3.8 mM. Sweep rate: 50 mV s^{-1} in pH 7.4, 50 mM phosphate buffer solution. (B,C) Nyquist plots of the various UOx/CNT electrodes as in (A). The electrolyte was pH 7.4, 50 mM phosphate buffer solution containing 10 mM $K_3[Fe(CN_6)]/K_4[Fe(CN)_6]$ (1:1).

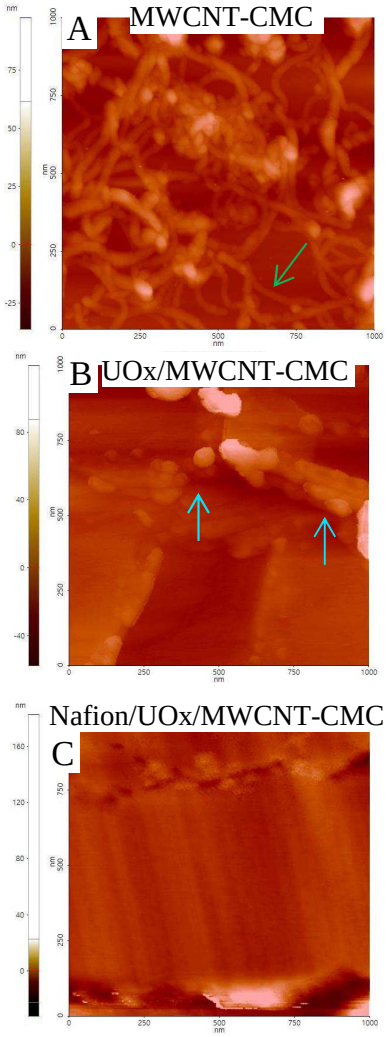

Fig. 2. AFM images of (A) MWCNT-CMC, (B) UOx/MWCNT-CMC, and (C) Nafion/UOx/MWCNT-CMC. Horizontal scale: 1 × 1 μm, Vertical scale: (A) 125 nm, (B) 200 nm, and (C) 200 nm.

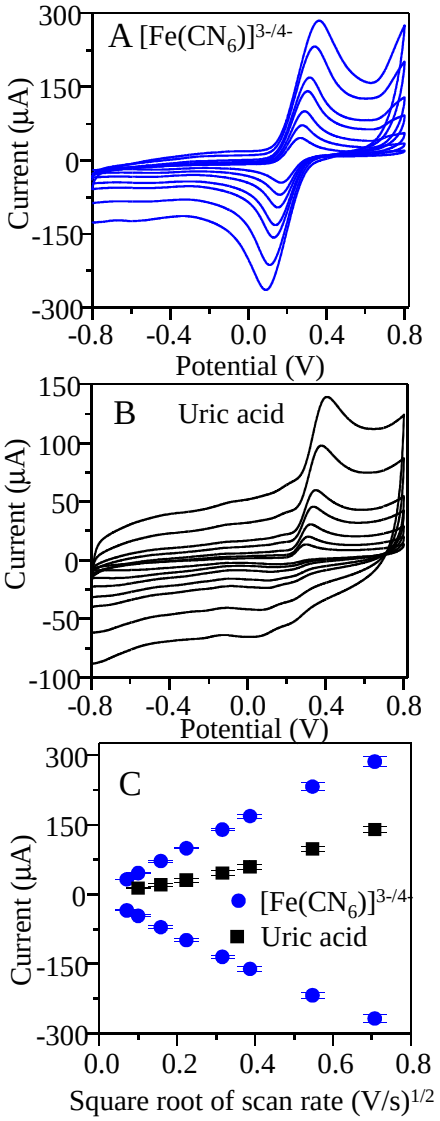

Fig. 3. CVs of (A) 3.8 mM uric acid and (B) 10 mM $K_3[Fe(CN_6)]/K_4[Fe(CN)_6]$ (1:1) with the UC/MWCNT-CMC Au electrode at various scan rates. Scan rates: 0.01, 0.025, 0.05, 0.10, 0.15, 0.30, and 0.50 V s^{-1}. (C) Dependence of peak current on square root of potential sweep rate with electrolyte in 50 mM phosphate buffer solution at pH 7.4.

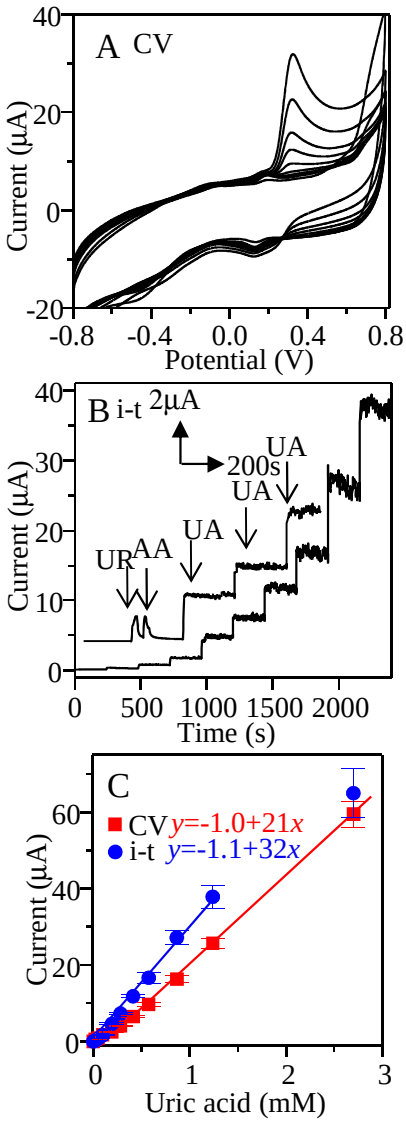

Fig. 4. (A) CV and (B) effects of interfering compounds with respect to the UOx/SWCNT-CMC/Au electrode. Sweep rate: 50 mV s^{-1}. Uric acid concentrations of 0, 0.020, 0.050, 0.10, 0.19, 0.28, 0.41, 0.58, 0.87, and 1.2 mM in pH 7.4 phosphate buffer solution (B). Inset: The effects of interferent species (0.1 mM urea (UR) and 0.1 mM ascorbic acid (AA)). The sequential concentrations of uric acid (UA) were 0.1, 0.2, and 0.4 mM. The polarization potential was +0.35 V vs. Ag/AgCl with an electrolyte of pH 7.4, 50 mM phosphate buffer solution. (C) Calibration plot for uric acid response using the data in 4A and 4B. The sensitivities of the electrodes were 233 μA mM^{-1} cm^{-2} (r = 0.999 in the linear range of 0.020-2.7 mM) by CV and 356 μA mM^{-1} cm^{-2} (r = 0.999 in the linear range of 0.020-1.2 mM) by CV.

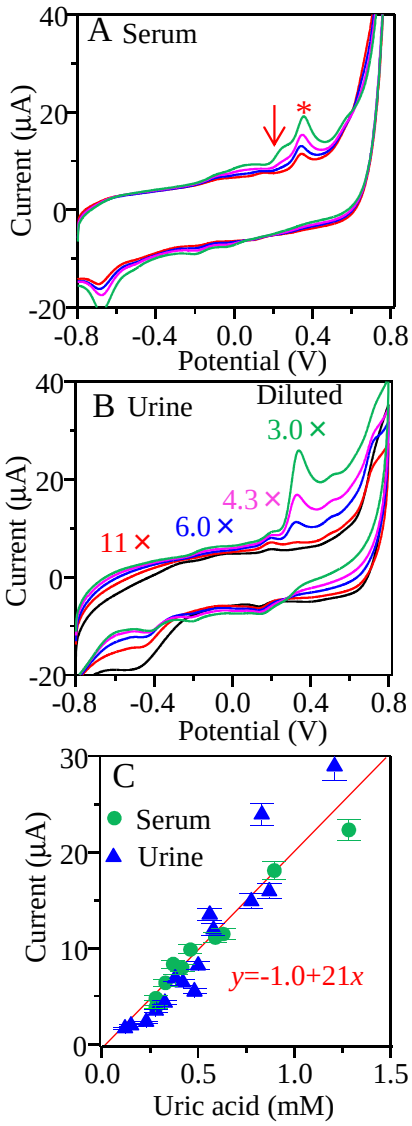

Fig. 5. (A) CV of serum sample. Uric acid concentrations of 0.28, 0.37, 0.46, and 0.63 mM. Sweep rate: 50 mV s^{-1}. (B) CV of urine sample with various dilutions. Raw urine concentration was 2.5 mM. Sweep rate: 50 mV s^{-1} in pH 7.4 phosphate buffer solution. (C) Plot of biosensor values (detection current) and enzymatic colorimetry kit values of various serums and urines. The fitting line is based on the standard sample in Fig. 4C.

Highlights

- Detection of clinically important uric acid in blood and urine is presented.
- Thin film biosensor composed of carbon nanotube and enzyme uricase is presented.
- Carbon nanotube is dispersed in aqueous solution with carboxymethylcellulose.